Heliyon 9 (2023) e20875

Contents lists available at ScienceDirect

Heliyon

journal homepage: www.cell.com/heliyon

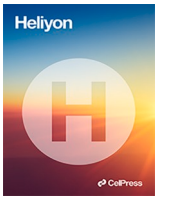

Study of the catalytic wet air oxidation of p-hydroxybenzoic acid on a fresh ruthenium catalyst supported by different oxides

Tijani Hammedi [a,*], Rahma Bensouilah [a,**], Abdelkader Ouakouak [b], Jordi Llorca [c], Francisco Medina Cabello [d], Zouhaier Ksibi [a]

[a] University of Tunis ElManar, Faculty of Sciences of Tunis, Laboratory of Materials Chemistry and Catalysis LR01ES08, Tunis, 2092, Tunisia
[b] Research Laboratory in Subterranean and Surface Hydraulics, University of Biskra, PO Box 145, Biskra, 07000, Algeria
[c] Universitat Politècnica de Catalunya, Institute of Energy Technologies, Catalysis and Energy Laboratory, Av. Diagonal 647, 08028, Barcelona, Spain
[d] Rovira i Virgili University, Chemical Engineering Department, Av/Països Catalans 26, 43007, Tarragona, Spain

ARTICLE INFO

Keywords:
CWAO
Ru catalysts
P-hydroxybenzoic acid
Support effects
Sol-gel processing

ABSTRACT

The catalytic wet air oxidation (CWAO) of p-hydroxybenzoic acid (p-HBA) was conducted in a batch reactor at 140 °C, and at a total air pressure of 50 bar over Ru-based catalysts. Four materials were selected as supports – TiO_2, CeO_2–TiO_2, ZrO_2–TiO_2, and La_2O_3–TiO_2 – all of which had mesopores in their texture and pollutant adsorption capacities. The supports were prepared by the sol-gel method, and then impregnated with 3 wt% of Ru precursor. Such characterization techniques as N_2-sorption, XRD, XPS, H_2–TPR, NH_3-TPD, TEM, and HAADF-STEM were used to analyze the different solids. The correlation between catalytic activities and physicochemical properties was discussed. A significant specific surface area (S_{BET}), a large amount of surface-active oxygen, and Lewis acidity sites were observed on cerium-containing catalysts (Ru/CeTi). Fresh Ru catalysts containing cerium showed higher activity than Ru/TiO_2, Ru/ZrTi, and Ru/LaTi catalysts. It is assumed that the acidic sites and surface oxygen trap the p-HBA molecule, thus increasing the catalytic properties of the Ru particles which interact with the surface oxygen through the cerium redox process (Ce^{3+}/Ce^{4+}). As the presence of cerium increases surface-active oxygen, it inhibits the deposition of carbon on the surface of the Ru catalyst. The pseudo-second order (PSO) model adequately described the kinetic data of the p-HBA oxidation reaction using Ru catalysts.

1. Introduction

One of the major global issues of our times is the decline in the quantity and quality of freshwater. The demand for freshwater is increasing as the world's population grows, making it a challenge for many countries to obtain an adequate supply. In addition, the distribution of water is geographically highly unequal, and some regions are near-desert, while a large proportion of water resources are relatively polluted [1].

Of the existing technologies that are currently available for wastewater purification, conventional biological treatment is the most

* Corresponding author.
** Corresponding author.
E-mail addresses: tijani.hammedi@fst.utm.tn (T. Hammedi), rahma.bensouilah@fst.utm.tn (R. Bensouilah).

https://doi.org/10.1016/j.heliyon.2023.e20875
Received 24 April 2023; Received in revised form 4 October 2023; Accepted 9 October 2023
Available online 11 October 2023

widely used, even though it requires large volumes and long residence times and is not feasible for wastewater containing growth-inhibiting microbial compounds. Meanwhile, wet air oxidation (WAO) is emerging as an effective technology for eliminating toxic, hazardous, and non-biodegradable industrial effluents into CO_2, H_2O, and N_2, under conditions of high temperature (125–320 °C) and pressure (50–200 bar), with air or oxygen as oxidant [2]. However, the implementation of this technology for industrial wastewater treatment is limited by its operating conditions and its high investment costs. Alternatively, the catalytic wet air oxidation (CWAO) process is a particularly suitable approach [3] because, among other advantages, it can treat extremely concentrated effluents in just a few hours without releasing hazardous gases or sludge. A catalyst, however, can effectively reduce the required operating conditions, increase the oxidation rate of the organic compounds and shorten the reaction time. Studies have shown that most of the catalysts used are based on precious metal. Indeed, supported noble metals (Pd, Pt, Ru, Ir and Rh) have proven effective for the removal of organic contaminants by catalytic wet air oxidation given their stability in aqueous medium [4,5]. These catalysts have the potential to be both stable and efficient for a wide variety of polluted effluents, including organic compounds [6]. However, most supported metal catalysts developed for CWAO show serious deactivation problems, because of (i) the leaching of the active phases, (ii) the deposition of carbonaceous species, which limit the accessibility of the reactants to the active phases, or (iii) the oxidation of the metallic phases, which become less active. One of the most active metals for this purpose is ruthenium, which has received considerable attention because it performs so well in the CWAO of compounds such as phenol, carboxylic acid and industrial wastewaters [7], but its activity seemed to be dependent on the nature and the texture of the support [8]. The most commonly used supports for these metals are CeO_2, TiO_2 and ZrO_2, used separately or in combination [9–11].

For industrial applications, much attention has been paid to the use of CWAO as an alternative technique for degrading the organic compounds generated by various industries that produce a range of harmful pollutants in wastewater. The following review focuses on p-hydroxybenzoic acid (p-HBA) taken as an industrial pollutant model molecule. p-HBA is the monomeric source of parabens, and is extensively used in pharmaceuticals and personal care products (PPCPs), varnishes, tobacco and animal feeds at industrial scale. In addition, it is very abundant in a wide variety of agro-industrial wastewaters (olive oil and table olive industries, distilleries, etc.). However, p-HBA is a non-biodegradable, widespread organic pollutant that is extremely toxic and poses a huge threat to aquatic organisms and human health, and is difficult to remove through conventional methods. Several studies have confirmed that p-HBA can have adverse effects on human health such as infertility in males and breast cancer in females [12,13].

In our earlier studies, p-HBA CWAO was investigated in a batch reactor using ruthenium catalysts supported by mixed oxides, namely CeO_2–TiO_2 [8,14] and CeO_2–Al_2O_3 [15]. The sol-gel method with the use of supercritical autoclave drying was employed to synthesize these mixed oxides. Indeed, this technology makes it possible to better control the metal particle size and catalyst porosity, and leads to considerable homogeneity among the various precursors [8]. As one of the most active metals for CWAO, Ru's activity remains dependent on support type and texture. In this study, ruthenium catalysts supported on TiO_2, ZrO_2–TiO_2, La_2O_3–TiO_2, and CeO_2–TiO_2 were systematically investigated and compared in the CWAO of p-HBA in a batch reactor, with the objective of understanding how they are affected by the structural and textural properties of the mixed oxide. The CWAO was studied by adding different amounts of Ce, Zr and La to the TiO_2 reference, with the optimum ratio between the two oxides being 16/74. These materials have the advantage of providing active sites for the adsorption and activation of organic compounds and facilitating their interaction with oxygen.

Thus, this study focuses on the interesting catalytic systems TiO_2, ZrO_2–TiO_2, La_2O_3–TiO_2, and CeO_2–TiO_2 in combination with the metal Ru. These supports were prepared by the sol–gel method and ruthenium nanoparticles (3.0 wt%) were impregnated to give 3Ru/TiO_2, 3Ru/Zr–Ti, 3Ru/La–Ti, and 3Ru/Ce–Ti catalysts. All the solids were characterized by nitrogen adsorption, XRD, H_2-TPR, NH_3-TPD, XPS, TEM and HAADF–STEM and their catalytic activities were evaluated in the CWAO of p-HBA in a batch reactor at 140 °C, and at a total air pressure of 50 bar. This study also intends to outline the oxidation kinetics of p-HBA acid.

2. Experimental section

2.1. Materials

Titanium (IV) isopropoxide ($Ti[OCH(CH_3)_2]_4$, 99.9 %), cerium(III) nitrate hexahydrate ($Ce(NO_3)_3.6H_2O$, 99 %), lanthanum (III) nitrate hexahydrate ($La(NO_3)_3.6H_2O$, 99 %), zirconium(IV) propoxide solution ($Zr(OCH_2CH_2CH_3)_4$, 70 wt % in 1-propanol), ethyl acetoacetate ($C_6H_{10}O_3$, 99 %), nitric acid (HNO_3, 65 %) and absolute ethanol (C_2H_5OH) were purchased from Sigma-Aldrich. Ruthenium (III) nitrosyl nitrate solution ($Ru(NO)(NO_3)_3$, 31.3 %) was purchased from Alfa Aesar. These reagents were used without further purification.

2.2. Preparation of supports and catalysts

In this study, TiO_2, CeO_2–TiO_2, La_2O_3–TiO_2 and ZrO_2–TiO_2 supports were synthesized by the sol-gel method as follows:

To prepare pure TiO_2, 3.8 ml of titanium (IV) isopropoxide was dissolved in 12.5 ml of anhydrous ethanol at room temperature. After stirring the solution for 20 min, 1.6 ml ethyl acetoacetate was added in order to control hydrolysis and condensation reaction rates. Once 30 min of magnetic stirring had elapsed, 2.25 ml of 0.1 M HNO_3 aqueous solution was added dropwise according to the molar ratio h = H_2O: Ti equal to 10. Agitated for 15–20 min, a transparent, homogeneous yellow gel was formed. Subsequently, the resulting gel was placed into an autoclave, dried under supercritical conditions of ethanol (P = 63 bars, T = 243 °C) to obtain aerogels, then calcined under oxygen at 500 °C for 3 h.

The binary oxides CeO_2–TiO_2, La_2O_3–TiO_2 and ZrO_2–TiO_2, with molar ratios Ce: Ti, La: Ti and Zr: Ti equal to 1:5, were prepared by

sol-gel method as follows. In the first preparation step, Cerium (III) nitrate hexahydrate (0.762 g), Lanthanum (III) nitrate hexahydrate (0.601 g) and Zirconium (IV) isopropoxide isopropanol (0.5 ml) were separately dissolved in absolute ethanol (8.7, 8 and 9.5 ml respectively).

Ru catalysts containing 3 wt% on various supports were prepared by incipient-wetness impregnation method. Ru(NO) $(NO_3)_3$ was dissolved in absolute ethanol and stirred for 60 min. A small amount of support (about 1 g support to 1 ml ethanol) was added to the solution. Once stirred vigorously for 3h, the impregnated solids were (i) dried at 90 °C for 12h under air, (ii) reduced under H_2 flow (30 ml min^{-1}) at 300 °C for 2 h and (iii) finally, passivated at room temperature under N_2 flow (30 ml min^{-1}) for 15 min. The treated catalysts were labelled as Ru/TiO_2, Ru/CeTi, Ru/ZrTi, and Ru/LaTi.

2.3. Catalyst characterization

The prepared solids were characterized by means of N_2 adsorption, XRD, H_2-TPR, NH_3-TPD, XPS, TEM and HAADF–STEM techniques. Nitrogen sorption measurements were performed using an ASAP 2020 Micromeritics instrument. The samples were outgassed under high vacuum at 200 °C for at least 5 h prior to measurement. The specific surface area was calculated by applying the BET (Brunauer, Emmett, and Teller) method, and the pore size distribution (measured from the desorption branch of the isotherm) was determined according to the BJH (Barrett, Joyner and Halenda) model. X-ray diffraction (XRD) analyses were performed using a Philips PW1050 diffractometer. The average crystallite size of the samples was estimated using the Debye-Scherrer equation. Hydrogen temperature-programmed reduction (H_2-TPR) profiles were obtained using a Micromeritics Autochem 2920 analyzer TPD/R/O linked to a thermal conductivity detector. The catalyst was treated under O_2(5 %)/He at 300 °C for 1 h and then reduced from 40 °C to 700 °C with H_2(5 %)/Ar (30 ml/min). High-angle annular dark-field scanning transmission electron microscopy (HAADF–-STEM) and energy dispersive X-ray analysis (EDX) were carried out at 200 kV with a Tecnai G2 F20 S-TWIN instrument equipped with a field emission electron source. The point-to-point resolution was 0.24 nm and the resolution between lines was 0.10 nm. X-ray photoelectron spectroscopy (XPS) was performed on a SPECS system equipped with an Al anode XR50 source operating at 150 mW and a Phoibos MCD-9 detector. The pass energy of the hemispherical analyzer was set at 25 eV and the energy step was set at 0.1 eV. The pressure in the analysis chamber was kept below 10^{-7} Pa.

2.4. Catalytic oxidation

CWAO of p-HBA acid was carried out in a 300 ml autoclave equipped with a magnetically driven stirrer to avoid any mass transfer limitation. A given mass of catalyst (500 mg) and 150 ml of p-HBA solution (10 mM) was used for each experiment [8,14]. After the reactor had been purged at least three times with N_2 to remove any trace of oxygen, it was heated to the desired reaction temperature (140 °C), and then synthetic air (20 vol% O_2 in N_2) or pure oxygen was introduced into the reactor to reach a total pressure of 50 bar. The stirrer was then switched on again. This time was considered as zero time for the reaction. Samples were collected regularly from the reactor to monitor the reaction. High-performance liquid chromatography (HPLC) was used to track the concentration of the starting reagent and reaction by-products. The HPLC system was equipped with a Hypersil Gold column and a UV-detector set at 254 nm. The mobile phase was an aqueous solution of ultra-pure water, acetonitrile and sulfuric acid (70/20/10) and the flow rate was set at 0.7 ml min^{-1}.

The turnover frequency (TOF) was calculated according to the Eq. (1):

$$TOF\left(s^{-1}\right) = \frac{[R_0] - [R_x]}{[R_0] * t_x} \tag{1}$$

where $[R_0]$ is the starting concentration of the reactant and t_x is the reaction time at x% consumption.

The pseudo-first-order (PFO) and pseudo-second-order (PSO) models were applied to depict the kinetic data in order to study the kinetic proprieties of p-HBA oxidation reaction. The non-linear forms of PFO and PSO models are given by the following Eq. (2) and Eq. (3)

$$q_t = q_e\left(1 - e^{-K_1 t}\right) \tag{2}$$

$$q_t = \frac{q_e^2 k_2 t}{1 + q_e k_2 t} \tag{3}$$

where, q_t and q_e (mmol/g) are the calculated and experimental values of oxidation capacity. k_1 and k_2 (L/min) are the rate constants.

3. Results and discussion

3.1. Characterization of catalysts

3.1.1. N_2-Physisorption measurements

The textural properties of the powdered samples were investigated by nitrogen physisorption at 77 K. Corresponding isotherms and BJH pore size distributions of the supports are presented in Fig. 1A(a-d) and 1B(a-d). According to the IUPAC classification [16], all the

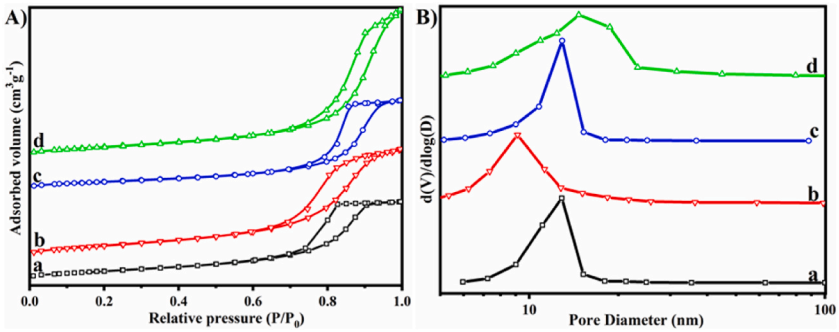

Fig. 1. (A) N_2 -sorption isotherms and (B) BJH pore distribution of (a) TiO_2, (b) CeTi, (c) ZrTi, and (d) LaTi supports.

Table 1
Physical properties and total H_2 consumptions of prepared catalysts.

Samples	S_{BET} ($m^2.g^{-1}$)	**Pore diameter (nm)**	TiO_2 crystallite size (nm)	Total H_2 Consumption (μmol/g)
TiO_2	82	13	10.7	85
CeTi	183	9.2	7.3	438
LaTi	160	15	7.7	243
ZrTi	131	13	30	293
Ru/TiO_2	80	14	11	230
Ru/CeTi	175	11	6.3	744
Ru/LaTi	101	9.3	8.5	260
Ru/ZrTi	105	15.5	25.2	313

samples show type IV isotherms, indicating the mesoporous structure of the samples. This type of isotherm is characterized by capillary condensation accompanied by an H_2 type hysteresis loop, for TiO_2, CeTi and ZrTi supports [Fig. 1A(a-d)], which is attributed to complex pore structures due to strong network effects. The LaTi support isotherm [Fig. 1A(d)] does not reach a plateau near $P/P_0 = 1$, which indicates larger mesopores. The Ru catalysts showed textural properties similar to those of the supports. Table 1 summarizes the main textural parameters of all samples. Pure TiO_2 exhibits a specific surface area of 82 m^2/g. The addition of Ce, La and Zr to the TiO_2 reference significantly increases the S_{BET} to 183, 160 and 131 m^2/g, respectively. The impregnation of 3 wt % of Ru on TiO_2, CeTi, LaTi and ZrTi supports shows a decrease in surface area, probably due to the blocking of mesopores by Ru particles.

3.1.2. X-Ray diffraction analysis

The XRD pattern results of the supports are depicted in Fig. 2(a–d). The pure TiO_2 XRD pattern [Fig. 2(a)] showed typical diffraction peaks indexed to the anatase phase (JCPDS no.: 88–1175), while no rutile phase was discernible. Intense diffraction peaks appearing at about 2θ (°) = 25.34, 37.9, 48.11, 54.02, 55.10, and 62.57 correspond to orientations (101), (004), (200), (105), (211), and (204), respectively. The ZrTi XRD pattern [Fig. 2(b)] uniquely reveals the TiO_2 phase. No crystalline phase of pure ZrO_2 was recorded in the spectrum of ZrTi support. The addition of zirconia stabilizes the anatase phase, as the rutile form could not be affected. Thus, indicating a homogeneous mixing of the Zr and Ti components in this sample. For the CeTi support [Fig. 2(c)], the diffraction peaks noted at 2θ (°) = 28.52 and 33.45 were attributed to the cubic CeO_2 but were broader and weaker than those of pure TiO_2, suggesting probably a good dispersion of its crystal phases. In the spectrum of the LaTi sample [Fig. 2(d)], the La_2O_3 phase was detected, and there was a single weaker signal at 2θ (°) = 30.37. The rest of the peaks belong to the TiO_2 phase. The XRD patterns of catalysts are not affected by the impregnation of ruthenium, as the diffraction peaks of metallic Ru and ruthenium oxide (Ruthenium, syn, PDF 06–0663: 2θ (°) = 38.39, 42.15 and 44.01) were not observed, which might be the result of the presence of highly dispersed ruthenium nanoparticles and the fact that the accessibility of Ru is poor on Ru (3.0 wt%) catalyst. There is a presence of rather large and discrete Ru particles on the surface of synthesized catalyst, as determined by HAADF-STEM measurements [Fig. 5], which reveals the presence of Ru particles in the range of 15–62 nm. A similar observation was noted by other researchers in the case of Ru/TiO_2–CeO_2 catalysts [14,17]. Table 1 displays the average TiO_2 crystallite size of all the investigated samples, determined by Debye-Scherrer relation (Eq. (4)) using 2θ and the full width at half maximum (FWHM) of the (hkl) peaks,

$$D = \frac{k\lambda}{\beta \cos\theta}(nm) \tag{4}$$

where D is the average crystallite size (nm), K is the shape factor (0.9), λ is the wavelength of X-ray (1.5406 Å) Cu Kα radiation, θ is the Bragg angle, and β is the corrected line broadening of the nanoparticles [18]. As shown in Table 1, ZrTi solid had the largest crystallite size of anatase TiO_2 (30 nm), which was consistent with XRD intensity.

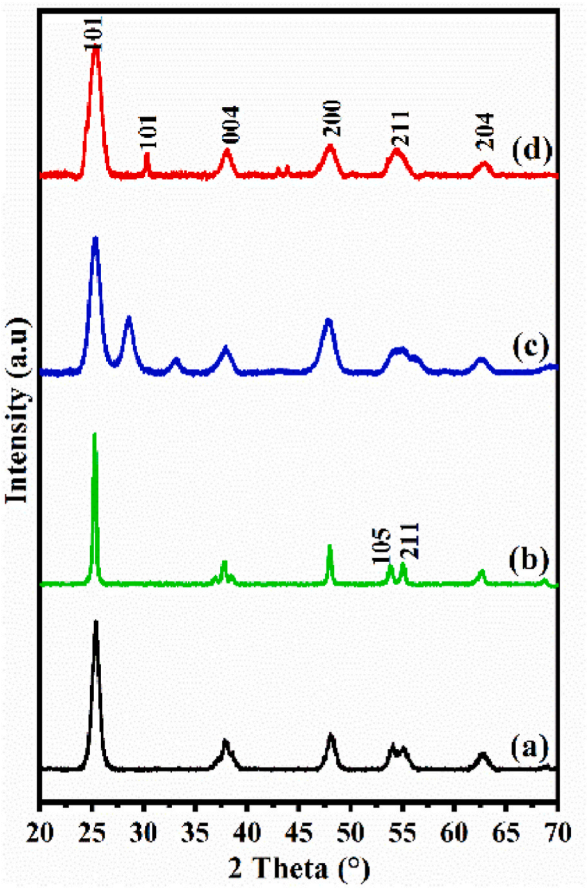

Fig. 2. XRD patterns of (a) TiO_2, (b) ZrTi, (c) CeTi and (d) LaTi supports.

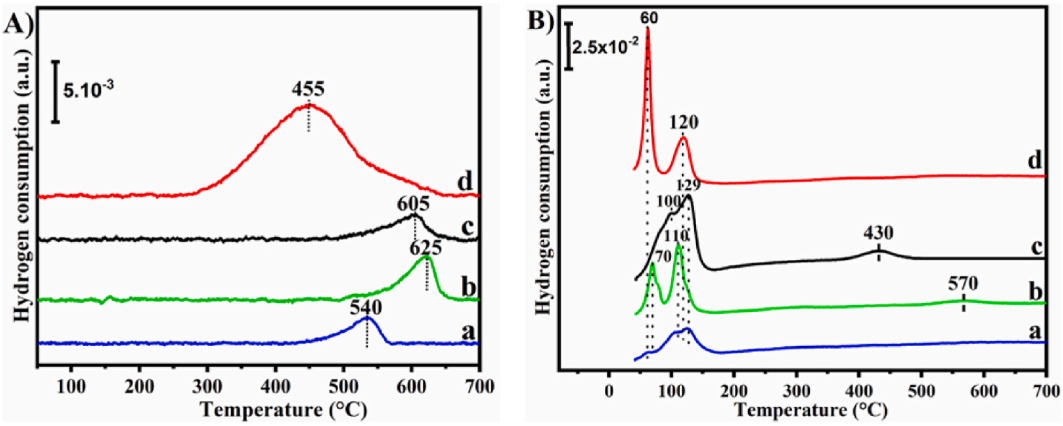

Fig. 3. H_2-TPR profiles of A: (a) TiO_2, (b) LaTi, (c) ZrTi, and (d) CeTi supports; and of B: (a) Ru/TiO_2, (b) Ru/ZrTi, (c) Ru/LaTi, and (d) Ru/CeTi catalysts.

3.1.3. H_2-TPR profiles

Temperature programmed reduction (H_2-TPR) analyses were performed for supports and Ru fresh catalysts to investigate their reducibility and possible metal-support interactions (SMSI) as displayed in Fig. 3A and B. Between 40 and 500 °C, no reduction peak was observed for pure TiO_2 [Fig. 3A(a)]. A broad weak peak at 540 °C with a H_2 consumption of 85 μmol/g could be associated to the reduction of bulk oxygen of TiO_2 as reported by Zhang et al. [19], suggesting that TiO_2 is difficult to reduce. In the TPR spectrum of the LaTi [Fig. 3A(b)] and ZrTi [Fig. 3A(c)] samples, the reduction behavior is similar, with only one reduction peak shifted to higher

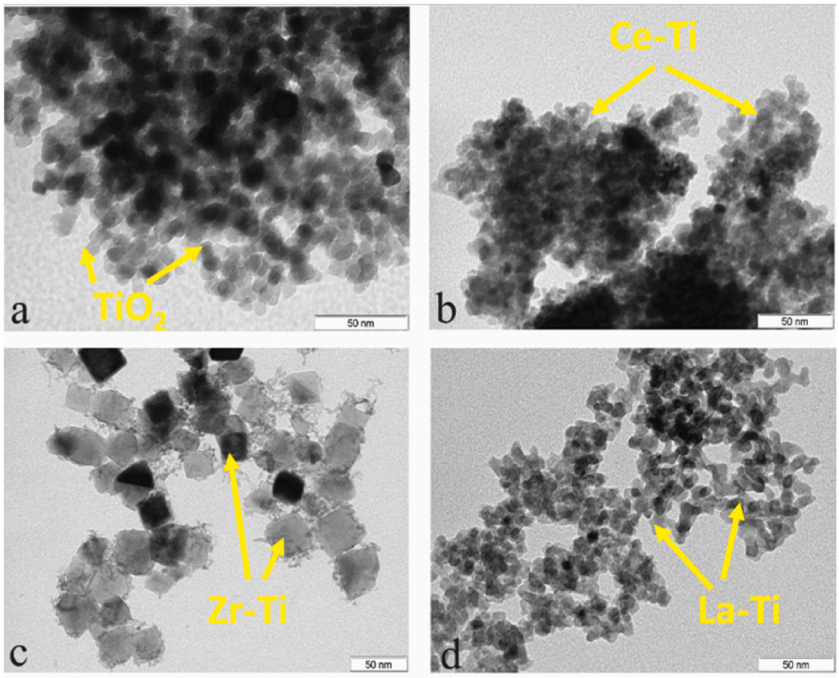

Fig. 4. TEM images of the sol-gel prepared supports (a) TiO_2, (b) CeTi, (c) ZrTi, and (d) LaTi.

temperatures (625 °C and 605 °C, respectively). The ZrTi and LaTi samples consumed 293 and 243 μmol/g of H_2, respectively. Notably, in the case of CeTi mixed oxides, the H_2-TPR profile was characterized by a narrower intense reduction peak at 350–550 °C, with a maximum at 455 °C and a H_2 uptake of 438 μmol/g, which can be attributed to the reduction of the surface oxygen species of ceria, indicative of relatively high lattice oxygen mobility [20–22]. Moreover, the CeO_2 bulk did not reduce in the temperature range 300–600 °C, only above 750 °C [23]. This meant that the interaction between Ce and Ti mixed oxides could have an important effect on the reducibility of the sample. This was followed by a change in the amount of easily reducible surface oxygen species of Ce^{4+}. In correlation with the S_{BET} and XRD results, CeTi may be reduced more easily because of its better dispersion of ceria and higher surface area. Fig. 3B shows H_2-TPR profiles for fresh Ru-supported catalysts. Similar behavior is observed for all the fresh Ru/TiO_2, Ru/CeTi, Ru/LaTi, and Ru/ZrTi catalysts. The addition of Ru to these mixed oxides facilitates the surface shell reduction step. Furthermore, the ruthenium particle reduction peaks are shifted toward lower temperatures. The lower the temperature reduction is, the stronger the reducibility of the catalyst. In the H_2-TPR spectrum of Ru/CeTi catalyst [Fig. 3B(d)] two reduction peaks were observed, with the maximum at a temperature of 60 and 120 °C, which corresponds to a total H_2 consumption of 744 μmol/g, as listed in Table 1. The origin of this spectrum can be linked to the ruthenium particle reduction process. It is well known that the small Ru particles are reduced at lower temperatures than the larger particles. The redox behavior studied by H_2-TPR demonstrates that Ru/CeTi has the best redox ability of the four catalysts. This is an indication that the average ruthenium particle in the Ru/CeTi catalyst is smaller than in the Ru/ZrTi, Ru/LaTi ~ Ru/TiO_2 catalysts. The trend is similar in the catalytic activities of these catalysts in the CWAO of p-HBA, which implies that ruthenium particles interacted with these mixed oxides and then increased the redox reaction. It was noted that the increase in the redox abilities of fresh Ru catalysts after the impregnation of Ru particles was in accordance with the results of STEM, TPD-NH_3, XPS, and the activity tests. According to Table 1, the total H_2 consumption of fresh Ru catalysts is greater than the H_2 consumed by the reduction of supports alone. The amount of the total H_2 consumption for the reduction of Ru interacting with the support is given in Table 1 and the results were found to be in the order Ru/CeTi > Ru/ZrTi > Ru/LaTi > Ru/TiO_2.

3.1.4. TEM and HAADF-STEM measurements

TEM images of supports are presented in Fig. 4(a–d). The TiO_2 sample [Fig. 4(a)] shows spherical titanium oxide particles of around 9 nm. The TEM images indicate that the addition of Ce, Zr, and La to TiO_2 seems to influence the morphology and size of mixed oxides. The TEM micrographs of the CeTi and LaTi solids [Fig. 4(b)–(d)] revealed well crystallized mixed oxide grains of approximately ~ 8 and 8.11 nm, respectively, while for the ZrTi support [Fig. 4(c)] the grain size increased to ~ 30 nm. Furthermore, the mean grain sizes of TiO_2 for the four supports were very close to those calculated using the Scherrer equation (see XRD results).

HAADF-STEM micrographs and the size distributions for three selected catalysts are presented in Fig. 5(a–f). The samples comprise support particles that are very homogeneous in size and Ru particles. The support particles mostly measure about 8–30 nm. These results are in good agreement with those shown by TEM. The representative EDX spectrum shown in Fig. 5(a) shows the occurrence of Ru in the bright area inside the black square in the image. The Cu signal is due to the TEM grid. As seen in Fig. 5(a), the Ru particles are present throughout the samples. The size distribution of the Ru particles on the Ru/CeTi catalyst [Fig. 2(a-b)] was 15–40 nm, most of

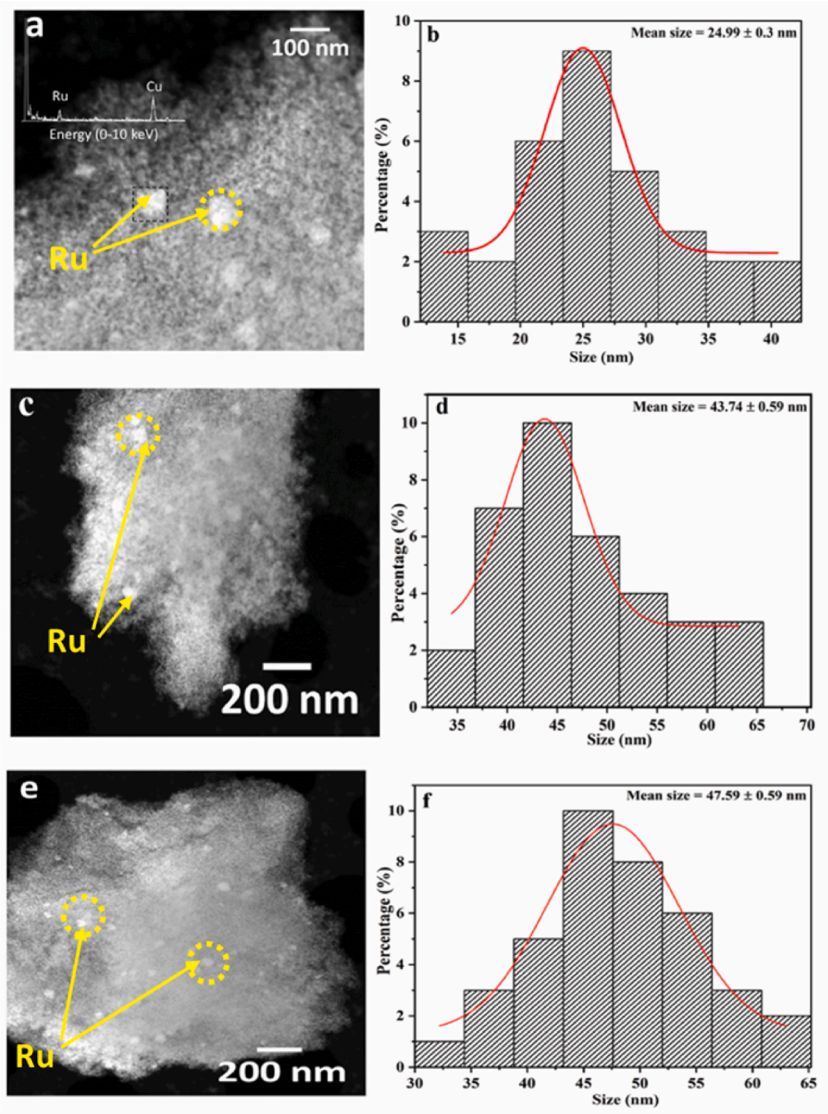

Fig. 5. HAADF-STEM images of (a) Ru/CeTi, (c) Ru/ZrTi, and (e) Ru/LaTi. Size distributions of (b)Ru/CeTi, (d)Ru/ZrTi, and (f) Ru/LaTi catalysts.

which were 20–30 nm, and on the Ru/ZrTi catalyst [Fig. 5(c-d)] 35–65 nm, most of which were 40–50 nm. The sizes of ruthenium particles on the Ru/LaTi catalyst [Fig. 5(e-f)] ranged from 30 to 65 nm, most of which were 45–55 nm, and their size distribution was in a broader range. The mean size of ruthenium particles on the CeTi support is smaller than those on the ZrTi and LaTi supports. The results suggest that the smallest Ru particles of 25 nm of the Ru/CeTi catalyst were the most active in the CWAO of p-HBA, which was also more acidic, as demonstrated by NH_3- TPD.

3.1.5. Ammonia thermodesorption

NH_3-TPD profiles of fresh Ru-supported catalysts are presented in Fig. 6. Temperature-programmed desorption of ammonia showed a broad desorption curve for Ru/LaTi [Fig. 6(a)] and Ru/ZrTi [Fig. 6(b)] catalysts, indicating that these samples have a broad acid site distribution. The maximum desorption peak for Ru/LaTi occurs at around 160 °C, whereas for Ru/ZrTi it occurs at around 230 °C. On the other hand, the high temperature desorption peak for Ru/CeTi [Fig. 6(c)] appears at 237 °C and is characteristic of materials with sharp acid site distribution. The highest peak of the NH_3-TPD spectra of the Ru/CeTi catalyst was higher than the peak of the other two catalysts, which indicated that the acid and base sites for this catalyst were strong. It is well-established that NH_3 adsorbs on strong acid sites (Brønsted or Lewis) and desorbs at high temperatures in a TPD experiment [24].

3.1.6. XPS results

XPS analysis was applied to study the chemical state of the surface of fresh Ru-supported catalysts. Table 2 lists the surface atomic

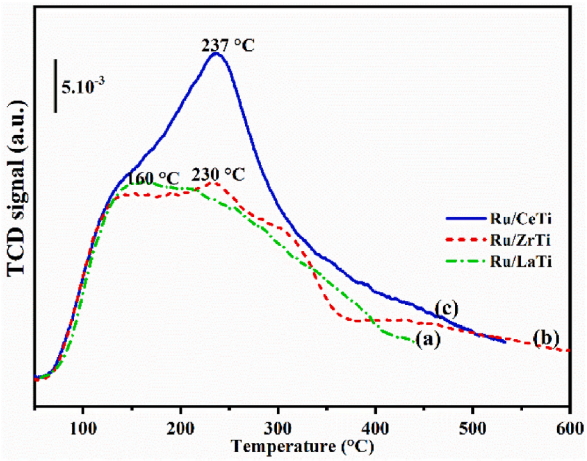

Fig. 6. NH_3-TPD of the (a) Ru/LaTi, (b) Ru/ZrTi, and (c) Ru/CeTi catalysts.

Table 2
XPS results of the fresh Ru-supported catalysts.

Catalysts	Atomic ratios		**Binding Energy (eV)**		O/O_t (%)	
	Ce, Zr, La/Ti	Ru/Ti	O_{sur}	O_{latt}	O_{sur}/O_t	O_{latt}/O_t
Ru/TiO_2	–	0.07	532.32	530.28	37.63	62.36
Ru/CeTi	0.73	0.16	532.40	530.06	62.66	37.33
Ru/LaTi	0.44	0.06	532.42	530.62	33.74	66.25
Ru/ZrTi	0.55	0.12	532.53	530.76	50.30	49.69

O_t: denotes the atomic concentration of the total oxygen.

ratio of various fresh Ru catalysts. The surface atomic composition of Zr, Ce and La is somewhat different from that of Ti. The Ce/Ti ratio in the Ru/CeTi sample (about 0.73) is higher than in the Zr/Ti sample (about 0.55) and the La/Ti sample (about 0.44). After the addition of Ce, Zr, and La to TiO_2, the changes in the concentration of Ru on the catalyst surface depended on the nature of the element loading. The Ru/Ti atomic ratio of the Ru/CeTi catalyst is generally higher than the Ru/Ti atomic ratio in the other three catalysts. The presence of Ce species created vacancies and unsaturated chemical bonds on the catalyst surface, thereby increasing adsorbed surface oxygen vacancies on the Ru/CeTi catalyst, perhaps because the higher surface oxygen of Ru/CeTi resulted in better catalytic activity in p-HBA degradation.

The O 1s XPS spectra of various catalysts are presented in Fig. 7(a–d). It should be noted that, after deconvolution of the O 1s peak, two oxygen species are identified for each catalyst, which is attributed to the surface oxygen vacancies (denoted by O_{sur}) with a binding energy of 532.32–532.53 eV, and lattice oxygen (denoted by O_{latt}) with a binding energy of 530.06–530.76 eV [22,25,26]. The addition of Ce, La and Zr to TiO_2 enhanced the peak intensities of O_{sur}. According to Table 2, the calculated O_{sur} ratio (62.66 %) of Ru/CeTi is much higher than that of Ru/TiO_2, Ru/LaTi and of Ru/ZrTi (37.63 %, 33.74 % and 50.30 %, respectively). However, the low activity over Ru/TiO_2 and Ru/LaTi in the CWAO of p-HBA might be associated with the low O_{sur} ratio. Surface adsorbed oxygen (O_{sur}) is reported to be more reactive in oxidation reactions because it is more mobile than lattice oxygen (O_{latt}) [25,27]. Consequently, the high surface adsorbed oxygen is beneficial for the CWAO reaction of p-HBA, and improves the activity of the catalysts. It should be mentioned that the results of the activity tests were consistent with this conclusion.

3.2. CWAO of p-hydroxybenzoic acid (p-HBA)

The catalytic performance of the synthetized catalysts was explored by using the catalytic wet air oxidation of p-HBA in aqueous medium at 140 °C and at a total air pressure of 50 bar with an HPLC apparatus. The complete oxidation of p-HBA produces only CO_2 and H_2O. However, if mineralization is not fully complete, some intermediates may be formed, as reported in our previous studies using similar catalysts [14,28]. The main by-products detected are phenol, hydroquinone and maleic acid.

The p-HBA conversions are plotted over time in the presence of supports and fresh Ru catalysts in Fig. 8(a–b). Before their catalytic efficiency was tested, a blank experiment (without a catalyst) was performed under the following reaction conditions: a temperature of 140 °C, a total air pressure of 50 bar and a time interval of 7 h. Fig. 8(a) shows that the conversion of p-HBA in the absence of a catalyst was very low (around 10 %) throughout the test. As for the catalytic activities of the supports, summary results for p-HBA conversion are shown in Fig. 8(a) and Table 3. The incorporation of ceria and zirconia into titania resulted in a higher catalytic activity as the p-HBA conversions gradually increased from 2.5 % (TiO_2 sample) to 19.2 and 19.6 % after 7 h for the ZrTi and CeTi samples, respectively. This means that the mixed oxide samples play a more significant role in enhancing activity than the corresponding TiO_2 single

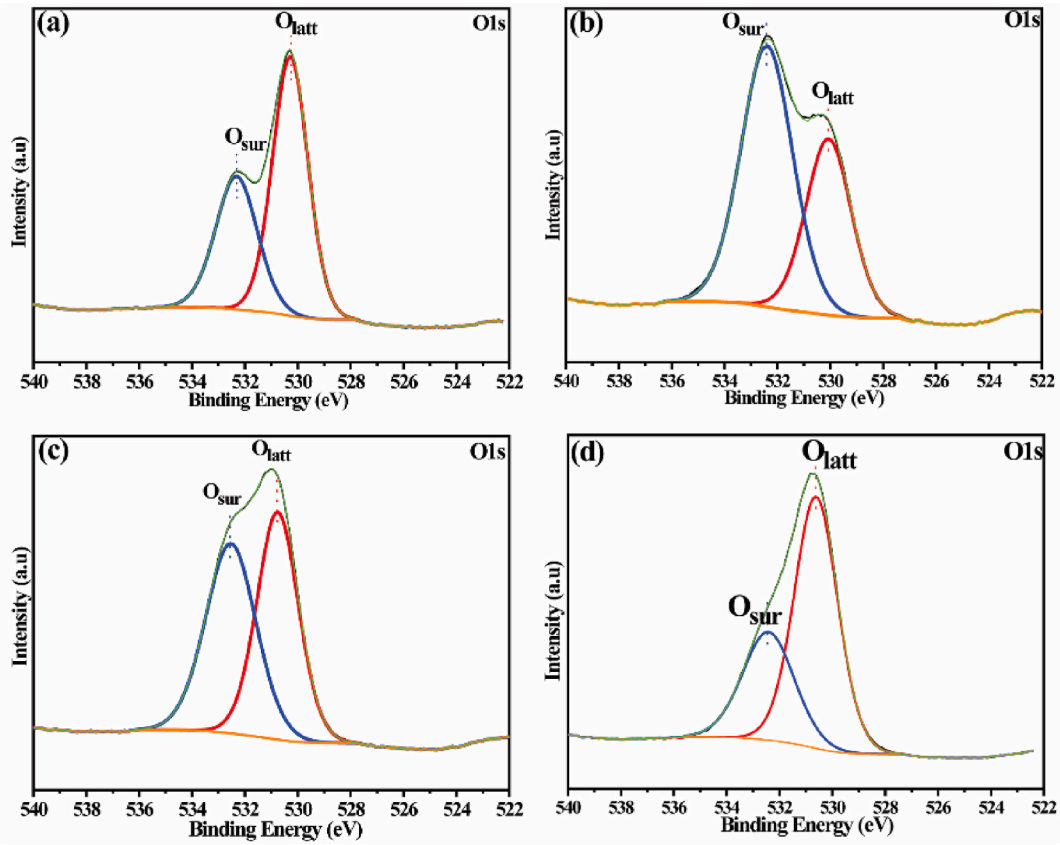

Fig. 7. XPS spectra of O 1s for (a) Ru/TiO_2, (b) Ru/CeTi, (c) Ru/ZrTi, and (d) Ru/LaTi catalysts.

oxide.

Fresh ruthenium catalysts showed higher p-HBA conversions than the supports [Fig. 8(b)]. Table 3 reports p-HBA conversions at 1 h and 7 h of reaction. As indicated, the conversion of p-HBA was considerably enhanced after Ru was added, and catalytic activity was high. The conversion of p-HBA on ruthenium supported on titania (Ru/TiO_2 catalyst) was 78 %, which is considerably higher than the 10 % conversion of the blank run (catalyst-free), [Fig. 8(b)]. Differences in catalyst/support activity at 7 h are around 30–50 %. Pre-reaction activity and conversion of p-HBA after 1 h and 7 h of reaction for the different Ru catalysts are summarized in Table 3. The Ru/ZrTi catalyst has a relatively high initial activity, with an initial reaction rate of 0.027 mmol $min^{-1}gcata^{-1}$ compared with the Ru/CeTi catalyst, whose initial rate is 0.016 mmol $min^{-1}g_{cata}^{-1}$. Moreover, the activity of Ru/CeTi catalyst is higher and a quasi-total p-HBA conversion is obtained after 6 h of reaction time. The Ru/TiO_2 and Ru/LaTi catalysts were less active than the Ru/CeTi and Ru/ZrTi catalysts, and the p-HBA conversion was 25 % and 27 % at 1 h of reaction, and then increased to 78 % and 74 % at 7 h of reaction, respectively. It was found that the addition of Ce and Zr to TiO_2 improves the activity of Ru catalysts. Thus, the catalytic activity of the samples was found in the following order when reacted for 7h: Ru/CeTi > Ru/ZrTi > Ru/LaTi ≈ Ru/TiO_2. Our results were consistent with those found by other authors. Triki et al. [15] studied the effect of Ru-supported on CeO_2–Al_2O_3, Al_2O_3, and CeO_2 on the catalytic oxidation of p-hydroxybenzoic acid, and the catalytic order was: Ru/Ce–Al > Ru/Al_2O_3 > Ru/CeO_2. Similarly, Minh et al. [29] studied the catalytic activities of Ru catalysts supported on commercial TiO_2 and ZrO_2 towards the CWAO of p-hydroxybenzoic acid. In their study, Ru/TiO_2 was the low activity catalyst at 140 °C and 50 bar of total air pressure. In our study, the fresh Ru-supported on mixed oxide CeTi was the most active catalyst in the CWAO of p-HBA: this means that catalytic activity may be influenced by the S_{BET} (180 m^2/g) and the synergic effect of the metal-support on the surface structural properties. Additionally, a larger catalyst surface (S_{BET}) promotes oxygen adsorption on its surface, which improves catalytic activity. Thus, the presence of ceria in the Ru/CeTi catalyst favors oxygen transfer and promotes a metal–support specific interaction, which is of great interest for CWAO applications. Besides, the interaction of Ru with the CeTi support creates labile oxygen species and has a strong influence on the catalytic activity of the catalyst. Previous studies [30,31] have shown that the metal-ceria interaction is a key factor in controlling catalyst performance, mainly in oxidation reactions. The results are confirmed by XPS data, which reveal that higher amounts of oxygen species were formed on the surface of Ru/CeTi because of its textural properties (mesoporous structure and large surface area), which could be another factor contributing to its enhanced activity for p-HBA CWAO.

Particle size may also have an effect since the results in Fig. 5(b)–(d) show that the Ru particle sizes of the Ru/CeTi and Ru/ZrTi catalysts are about 25 and 43 nm, respectively, and that Ru/CeTi is the most active for p-HBA CWAO. The small particle size obtained

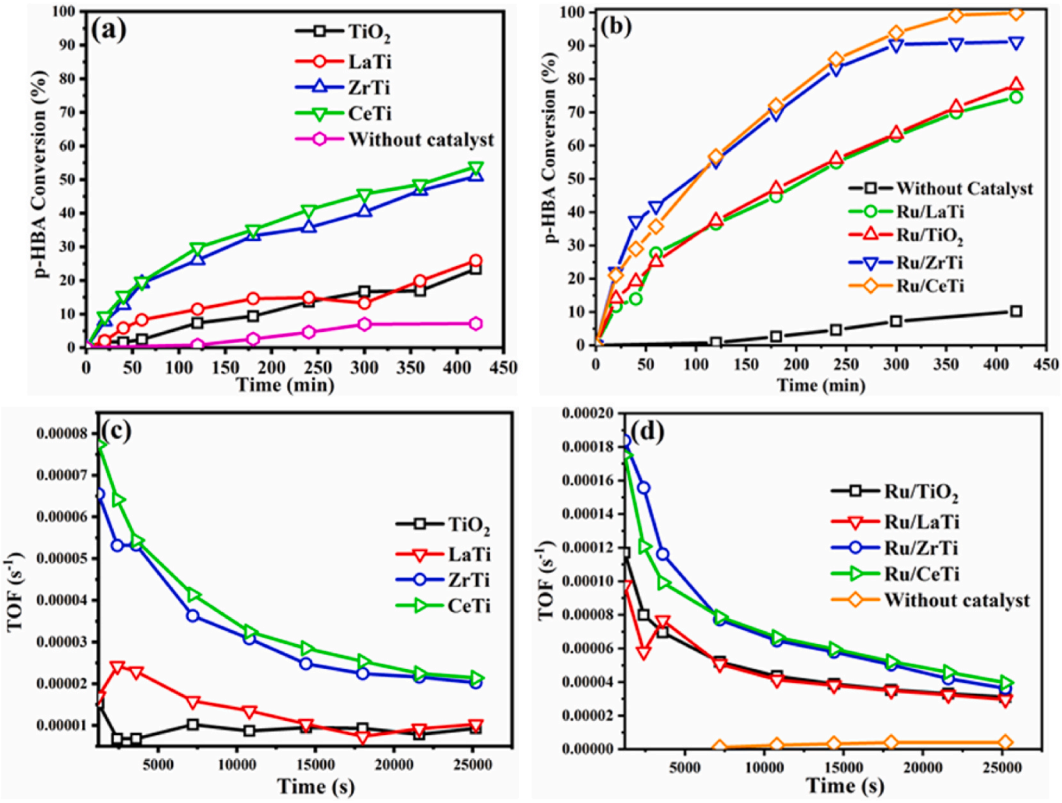

Fig. 8. CWAO of p-HBA. (a) Supports alone, (b) Fresh Ru-supported catalysts, and turnover frequency of (c) supports alone, (d) Fresh Ru-supported catalysts. [Reaction conditions (batch reactor): 140 °C, 50 bar of air, 150 ml of aqueous solution, p-HBA concentration: 10 mM (5 g L^{-1}), catalyst: 500 mg].

Table 3
Activity of fresh Ru-supported catalysts in CWAO of p-HBA acid.

Samples	**Initial activity (mmol $min^{-1}g_{cata}^{-1}$)**	p-HBA conversion (%) at	
		1h	7h
TiO_2	0.001	2.5	23
CeTi	0.011	19.6	54
ZrTi	0.009	19.2	51
LaTi	0.004	8.26	26
Ru/TiO_2	0.013	25	78
Ru/CeTi	0.016	36	100
Ru/LaTi	0.009	27	74
Ru/ZrTi	0.027	42	91

on the CeTi support could be due to the high S_{BET}. Besides, the catalytic properties may be correlated with the acidic properties. It appears that the Ru/CeTi catalyst is the most acidic, as demonstrated by NH_3-TPD. Lewis acid sites minimize polymer formation and hence carbon deposition.

The variation in turnover frequency (TOF) during p-HBA CWAO in the presence of the prepared materials is shown in Fig. 8(c)–(d). The TOF decreases as a function of reaction time. Its values reveal that Ru/CeTi and Ru/ZrTi are the most active catalysts, which is in good agreement with the evolution (over time) of p-HBA conversion.

The observed catalytic properties for the oxidation of p-HBA can be explained by the orientation of the p-HBA molecules on the catalyst surface. This orientation is determined by the redox and acid properties of the solid. Two main reasons can be proposed for correlating catalyst surface properties with p-HBA molecule orientation and, thus, the selectivity. These are presented in Fig. 9.

3.3. Kinetic behaviors

The effect of stirring time on the evolution of the p-HBA oxidation reaction was investigated in order to select the best model to

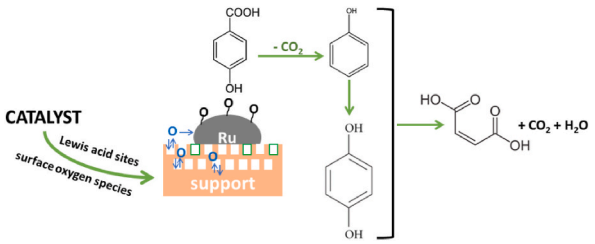

Fig. 9. Schematic representation of the adsorption mode of p-HBA acid depending on the surface oxygen species and the acid sites of the catalyst.

Table 4
Relevant parameters of the oxidation kinetics of p-HBA acid contaminants using the different mixed oxide supports.

Models	Catalyst	qe exp (mmol/g)	qe cal (mmol/g)	K_1 (L/min)	R^2	Chi-square test (χ^2)
PFO	TiO_2	0.61	1.14	0.002	0.981	0.001
	LaTi	0.76	0.81	0.004	0.941	0.004
	ZrTi	1.50	1.53	0.006	0.979	0.006
	CeTi	1.58	1.59	0.007	0.987	0.004
				K_2 (g/min. mg)		
PSO	TiO_2	0.61	0.322	0.001	0.083	0.057
	LaTi	0.76	0.390	0.001	0.187	0.046
	ZrTi	1.50	2.079	0.002	0.964	0.006
	CeTi	1.58	2.118	0.003	0.971	0.004

Table 5
Relevant parameters of the oxidation kinetics of p-HBA acid contaminants using Ru catalysts.

Models	Catalyst	qe exp (mmol/g)	qe cal (mmol/g)	K_1 (L/min)	R^2	Chi-square test (χ^2)
PFO	Ru/TiO_2	7.43	8.18	0.005	0.984	0.114
	Ru/LaTi	6.74	7.58	0.005	0.985	0.090
	Ru/ZrTi	8.94	9.06	0.009	0.977	0.250
	Ru/CeTi	9.79	10.44	0.007	0.991	0.110
				K_2 (g/min. mg)		
PSO	Ru/TiO_2	7.43	11.48	3.4×10^{-4}	0.989	0.078
	Ru/LaTi	6.74	10.76	3.5×10^{-4}	0.989	0.067
	Ru/ZrTi	8.94	11.34	8.5×10^{-4}	0.987	0.148
	Ru/CeTi	9.79	14.03	4.2×10^{-4}	0.994	0.081

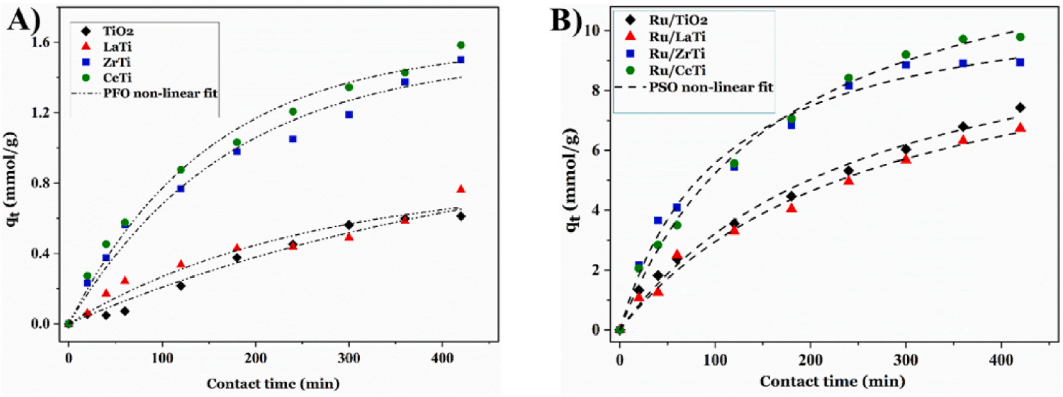

Fig. 10. (A) Fitting plots of the PFO kinetic model of p-HBA oxidation using the supports and (B) Fitting plots of the PSO kinetic model of p-HBA oxidation using the fresh Ru catalysts (m = 500 mg, V = 150 ml, pH ≈ 3.25).

describe the kinetic data for this reaction, performed in the presence of the prepared supports and Ru catalysts. The pseudo-first-order (PFO) and pseudo-second-order (PSO) models were widely applied to represent the data time-dependence experiments. The relevant parameters determining the kinetics of p-HBA oxidation using the studied catalysts are summarized in Tables 4 and 5.

According to the correlation coefficient (R^2) and chi-square test (χ^2) calculation, the PFO [Fig. 10A] fit the experimental data better

than the PSO (Fig. not shown) model for supports alone. Furthermore, the oxidation rate results (qe; mmol/g) show that the theoretical values (qe_{cal}) are in good agreement with the experimental ones (qe_{exp}) when the PSO model equation is used. However, in the case of Ru catalysts, the PSO equation gives the best fit for the kinetic data [Fig. 10B].

4. Conclusion

Ru catalysts successfully prepared by sol-gel and impregnation approaches have shown excellent catalytic activity in the CWAO reaction of p-HBA, with the following order of catalytic activity: Ru/CeTi > Ru/ZrTi > Ru/LaTi ≈ Ru/TiO_2. In addition, the conversion of p-HBA reached 100 % with Ru/CeTi after 6 h of reaction. The physicochemical characterization of the solids has revealed many interesting properties that explain their catalytic performances. However, mesoporous structure, acidic sites and high surface adsorbed oxygen are the most important factors that affect Ru/CeTi efficiency. Indeed, the presence of Ce species could create vacancies and unsaturated chemical bondings on the catalyst surface, resulting in increased adsorbed oxygen vacancies on the Ru/CeTi catalyst surface.

Data availability

Data will be made available on request.

CRediT authorship contribution statement

Tijani Hammedi: Conceptualization, Data curation, Formal analysis, Investigation, Methodology, Writing – original draft, Writing – review & editing, Software, Visualization. **Rahma Bensouilah:** Data curation, Investigation, Software, Writing – review & editing. **Abdelkader Ouakouak:** Data curation, Formal analysis, Software. **Jordi Llorca:** Data curation, Formal analysis. **Francisco Medina Cabello:** Data curation, Supervision, Validation, Writing – review & editing, Formal analysis, Resources. **Zouhaier Ksibi:** Project administration, Supervision, Validation, Resources.

Declaration of competing interest

The authors declare that they have no known competing financial interests or personal relationships that could have appeared to influence the work reported in this paper.

Acknowledgements

The authors would like to acknowledge the Ministry of Higher Education and Scientific Research of Tunisia (MESRS) for its financial support and express their deep gratitude to Prof. Jordi Llorca and Prof. Francisco Medina Cabello for their contributions through the different characterization analyses to successfully complete this study.

References

[1] M.A. Oturan, J.-J. Aaron, Advanced oxidation processes in water/wastewater treatment: principles and applications, Rev. Crit. Rev. Environ. Sci. Technol. 44 (23) (2014) 2577–2641, https://doi.org/10.1080/10643389.2013.829765.
[2] A.E. de Los Monteros, G. Lafaye, A. Cervantes, G. Del Angel, J. Barbier Jr., G. Torres, Catalytic wet air oxidation of phenol over metal catalyst (Ru, Pt) supported on TiO_2–CeO_2 oxides, Catal. Today 258 (2015) 564–569, https://doi.org/10.1016/j.cattod.2015.01.009.
[3] A. Cybulski, Catalytic wet air oxidation: are monolithic catalysts and reactors feasible? Ind. Eng. Chem. Res. 46 (12) (2007) 4007–4033, https://doi.org/10.1021/ie060906z.
[4] S. Keav, J. Barbier, D. Duprez, Deactivation and regeneration of wet air oxidation catalysts, Catal. Sci. Technol. 1 (3) (2011) 342–353, https://doi.org/10.1039/C0CY00085J.
[5] J. Mikulová, J. Barbier Jr., S. Rossignol, D. Mesnard, D. Duprez, C. Kappenstein, Wet air oxidation of acetic acid over platinum catalysts supported on cerium-based materials: influence of metal and oxide crystallite size, J. Catal. 251 (1) (2007) 172–181, https://doi.org/10.1016/j.jcat.2007.07.008.
[6] L. Oliviero, J. Barbier Jr., D. Duprez, A. Guerrero-Ruiz, B. Bachiller-Baeza, I. Rodrıguez-Ramos, Catalytic wet air oxidation of phenol and acrylic acid over Ru/C and Ru–CeO_2/C catalysts, Appl. Catal. B Environ. 25 (4) (2000) 267–275, https://doi.org/10.1016/S0926-3373(99)00141-1.
[7] D.P. Minh, P. Gallezot, M. Besson, Treatment of olive oil mill wastewater by catalytic wet air oxidation: 3. Stability of supported ruthenium catalysts during oxidation of model pollutant p-hydroxybenzoic acid in batch and continuous reactors, Appl. Catal. B Environ. 75 (1–2) (2007) 71–77, https://doi.org/10.1016/j.apcatb.2007.03.015.
[8] T. Hammedi, M. Triki, Z. Ksibi, A. Ghorbel, F. Medina, Comparative study of textural, structural and catalytic properties of xerogels and aerogels CeO_2–TiO_2 mixed oxides, J. Porous Mater. 22 (4) (2015) 939–948, https://doi.org/10.1007/s10934-015-9967-z.
[9] A. Pintar, J. Batista, T. Tišler, Catalytic wet-air oxidation of aqueous solutions of formic acid, acetic acid and phenol in a continuous-flow trickle-bed reactor over Ru/TiO_2 catalysts, Appl. Catal. B Environ. 84 (1–2) (2008) 30–41, https://doi.org/10.1016/j.apcatb.2008.03.001.
[10] S. Yang, Y. Feng, J. Wan, W. Zhu, Z. Jiang, Effect of CeO_2 addition on the structure and activity of RuO_2/γ-Al_2O_3 catalyst, Appl. Surf. Sci. 246 (1–3) (2005) 222–228, https://doi.org/10.1016/j.apsusc.2004.11.013.
[11] M.L. Rocha, G. Del Ángel, G. Torres-Torres, A. Cervantes, A. Vázquez, A. Arrieta, J. Beltramini, Effect of the Pt oxidation state and Ce^{3+}/Ce^{4+} ratio on the Pt/TiO_2-CeO_2 catalysts in the phenol degradation by catalytic wet air oxidation (CWAO), Catal. Today 250 (2015) 145–154, https://doi.org/10.1016/j.cattod.2014.09.016.
[12] L.E. Dodge, K.E. Kelley, P.L. Williams, M.A. Williams, S. Hernández-Díaz, S.A. Missmer, R. Hauser, Medications as a source of paraben exposure, Reprod. Toxicol. 52 (2015) 93–100, https://doi.org/10.1016/j.reprotox.2015.02.002.
[13] K. Nowak, W. Ratajczak–Wrona, M. Górska, E. Jabłońska, Parabens and their effects on the endocrine system, Mol. Cell. Endocrinol. 474 (2018) 238–251, https://doi.org/10.1016/j.mce.2018.03.014.

[14] T. Hammedi, M. Triki, M.G. Alvarez, R.J. Chimentao, Z. Ksibi, A. Ghorbel, J. Llorca, F. Medina, Total degradation of p-hydroxybenzoic acid by Ru-catalysed wet air oxidation: a model for wastewater treatment, Environ. Chem. Lett. 13 (4) (2015) 481–486, https://doi.org/10.1007/s10311-015-0529-z.
[15] M. Triki, Z. Ksibi, A. Ghorbel, F. Medina, Preparation and characterization of CeO_2–Al_2O_3 aerogels supported ruthenium for catalytic wet air oxidation of p-hydroxybenzoic acid, J. Sol. Gel Sci. Technol. 59 (1) (2011) 1–6, https://doi.org/10.1007/s10971-011-2452-5.
[16] M. Thommes, K. Kaneko, A.V. Neimark, J.P. Olivier, F. Rodriguez-Reinoso, J. Rouquerol, K.S. Sing, Physisorption of gases, with special reference to the evaluation of surface area and pore size distribution (IUPAC Technical Report), Pure Appl. Chem. 87 (9–10) (2015) 1051–1069, https://doi.org/10.1515/pac-2014-1117.
[17] M. Triki, Z. Ksibi, A. Ghorbel, F. Medina, Preparation and characterization of CeO_2–TiO_2 support for Ru catalysts: application in CWAO of p-hydroxybenzoic acid, Microporous Mesoporous Mater. 117 (1–2) (2009) 431–435, https://doi.org/10.1016/j.micromeso.2008.07.019.
[18] P. Praveen, G. Viruthagiri, S. Mugundan, N. Shanmugam, Structural, optical and morphological analyses of pristine titanium di-oxide nanoparticles–Synthesized via sol–gel route, Spectrochim. Acta Mol. Biomol. Spectrosc. 117 (2014) 622–629, https://doi.org/10.1016/j.saa.2013.09.037.
[19] C. Zhang, H. He, K.-i. Tanaka, Catalytic performance and mechanism of a Pt/TiO_2 catalyst for the oxidation of formaldehyde at room temperature, Appl. Catal. B Environ. 65 (1–2) (2006) 37–43, https://doi.org/10.1016/j.apcatb.2005.12.010.
[20] X. Wang, D. Liu, J. Li, J. Zhen, H. Zhang, Clean synthesis of Cu_2O@CeO_2 core@shell nanocubes with highly active interface, NPG Asia Mater. 7 (1) (2015), https://doi.org/10.1038/am.2014.128.
[21] I. Atribak, A. Bueno-López, A. García-García, Combined removal of diesel soot particulates and NOx over CeO_2–ZrO_2 mixed oxides, J. Catal. 259 (1) (2008) 123–132, https://doi.org/10.1016/j.jcat.2008.07.016.
[22] X. Gao, Y. Jiang, Y. Fu, Y. Zhong, Z. Luo, K. Cen, Preparation and characterization of CeO2/TiO2 catalysts for selective catalytic reduction of NO with NH_3, Catal. Commun. 11 (5) (2010) 465–469, https://doi.org/10.1016/j.catcom.2009.11.024.
[23] Y. Jiang, X. Wang, C. Bao, S. Huang, X. Zhang, X. Wang, Poisoning effect of CaO on CeO2/TiO2 catalysts for selective catalytic reduction of NO with NH_3, Kor. J. Chem. Eng. 34 (6) (2017) 1874–1881, https://doi.org/10.1007/s11814-017-0085-2.
[24] A. Chareonlimkun, V. Champreda, A. Shotipruk, N. Laosiripojana, Catalytic conversion of sugarcane bagasse, rice husk and corncob in the presence of TiO_2, ZrO_2 and mixed-oxide TiO_2–ZrO_2 under hot compressed water (HCW) condition, Bioresour. Technol. 101 (11) (2010) 4179–4186, https://doi.org/10.1016/j.biortech.2010.01.037.
[25] Y. Jiang, Z. Xing, X. Wang, S. Huang, X. Wang, Q. Liu, Activity and characterization of a Ce–W–Ti oxide catalyst prepared by a single step sol–gel method for selective catalytic reduction of NO with NH_3, Fuel 151 (2015) 124–129, https://doi.org/10.1016/j.fuel.2015.01.061.
[26] Y. Jiang, Z. Xing, X. Wang, S. Huang, Q. Liu, J. Yang, MoO_3 modified CeO_2/TiO_2 catalyst prepared by a single step sol–gel method for selective catalytic reduction of NO with NH_3, J. Ind. Eng. Chem. 29 (2015) 43–47, https://doi.org/10.1016/j.jiec.2015.04.023.
[27] W. Shan, F. Liu, H. He, X. Shi, C. Zhang, A superior Ce-W-Ti mixed oxide catalyst for the selective catalytic reduction of NOx with NH_3, Appl. Catal. B Environ. 115 (2012) 100–106, https://doi.org/10.1016/j.apcatb.2011.12.019.
[28] M. Triki, D.P. Minh, Z. Ksibi, A. Ghorbel, M. Besson, Ruthenium catalysts supported on TiO_2 prepared by sol–gel way for p-hydroxybenzoic acid wet air oxidation, J. Sol. Gel Sci. Technol. 48 (2008) 344–349, https://doi.org/10.1007/s10971-008-1827-8.
[29] D.P. Minh, G. Aubert, P. Gallezot, M. Besson, Degradation of olive oil mill effluents by catalytic wet air oxidation: 2-Oxidation of p-hydroxyphenylacetic and p-hydroxybenzoic acids over Pt and Ru supported catalysts, Appl. Catal. B Environ. 73 (3–4) (2007) 236–246, https://doi.org/10.1016/j.apcatb.2006.12.014.
[30] A. Trovarelli, Catalytic properties of ceria and CeO_2-containing materials, Catal. Rev. 38 (4) (1996) 439–520, https://doi.org/10.1080/01614949608006464.
[31] S. Imamura, Y. Okumura, T. Nishio, K. Utani, Y. Matsumura, Wet-oxidation of a model domestic wastewater on a Ru/Mn/Ce composite catalyst, Ind. Eng. Chem. Res. 37 (3) (1998) 1136–1139, https://doi.org/10.1021/ie970538m.